Cell Reports, Volume *38*

Supplemental information

The BTB transcription factors ZBTB11 and ZFP131 maintain pluripotency by repressing pro-differentiation genes

Görkem Garipler, Congyi Lu, Alexis Morrissey, Lorena S. Lopez-Zepeda, Yingzhen Pei, Simon E. Vidal, Ana Paula Zen Petisco Fiore, Begüm Aydin, Matthias Stadtfeld, Uwe Ohler, Shaun Mahony, Neville E. Sanjana, and Esteban O. Mazzoni

Figure S1

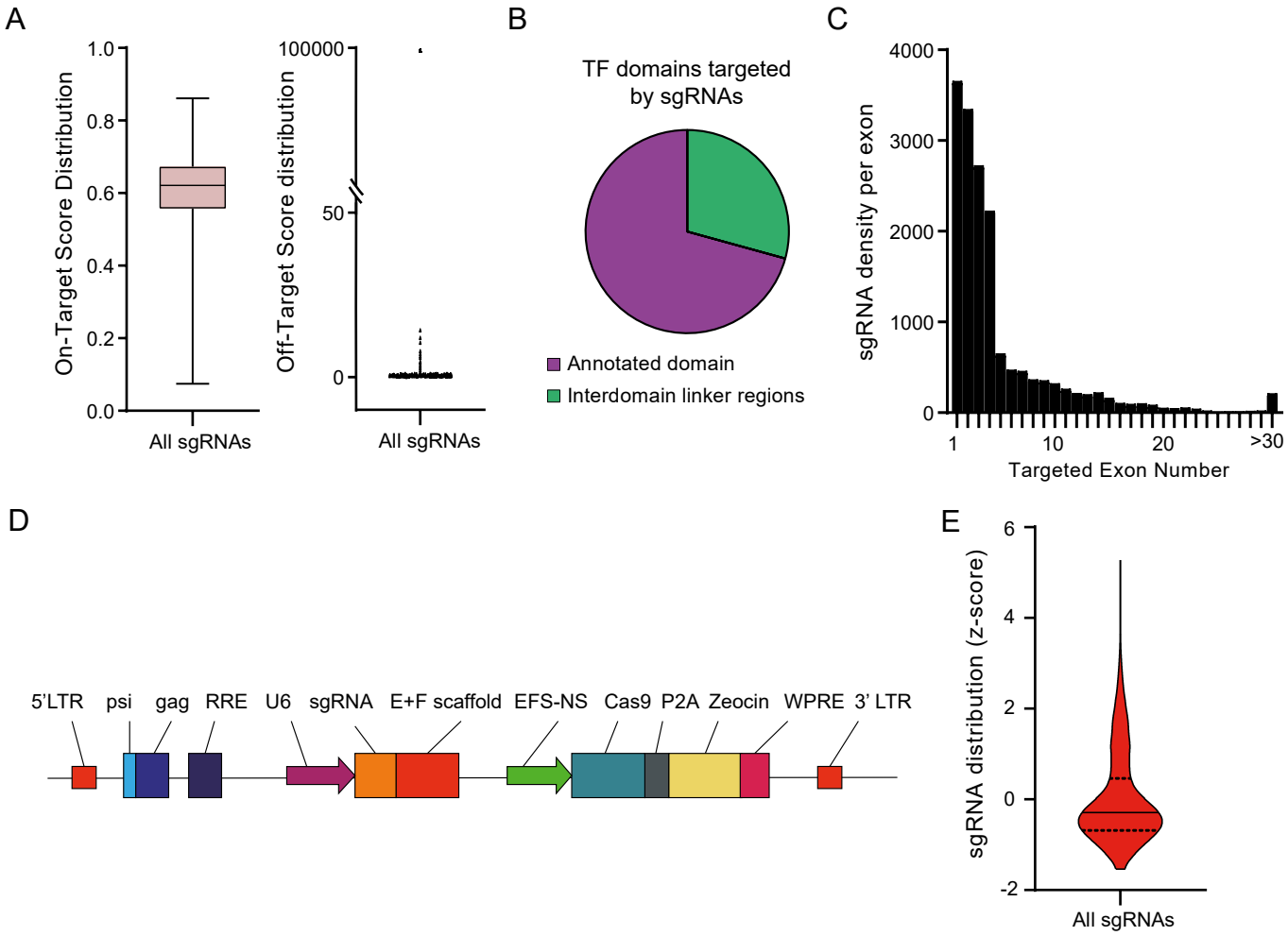
A
On-Target Score Distribution
1.0
0.8
0.6
0.4
0.2
0.0
All sgRNAs
Off-Target Score distribution
100000
50
0
All sgRNAs
B
TF domains targeted by sgRNAs
Annotated domain
Interdomain linker regions
C
sgRNA density per exon
4000
3000
2000
1000
0
1
10
20
>30
Targeted Exon Number
D
5'LTR
psi
gag
RRE
U6
sgRNA
E+F scaffold
EFS-NS
Cas9
P2A
Zeocin
WPRE
3' LTR
E
sgRNA distribution (z-score)
6
4
2
0
-2
All sgRNAs

Figure S1. CRISPR TF library targets 1682 TFs in the mouse genome.

(A) On-target and off-target score distribution of all sgRNAs in the library based on the GUIDES algorithm.

(B) Percentage of targeted annotated TF domains in the library based on Pfam. 71% of the sgRNAs target an annotated functional domain.

(C) Exon targeting density of sgRNAs in the library. sgRNAs were designed to target 5' exons to increase the chance of generating a frameshift.

(D) The lentiviral expression vector for sgRNA and Cas9. psi+, Psi packaging signal; RRE, Rev response element; EFS, elongation factor 1a short promoter; P2A, 2A self-cleaving peptide; WPRE, post-transcriptional regulatory element.

(E) Representation of the normalized number of reads of sgRNAs in the plasmid library with Z-score distribution. The solid line represents the mean z-score. Dashed lines represent quartiles.

Related to Figure 1.

Figure S2

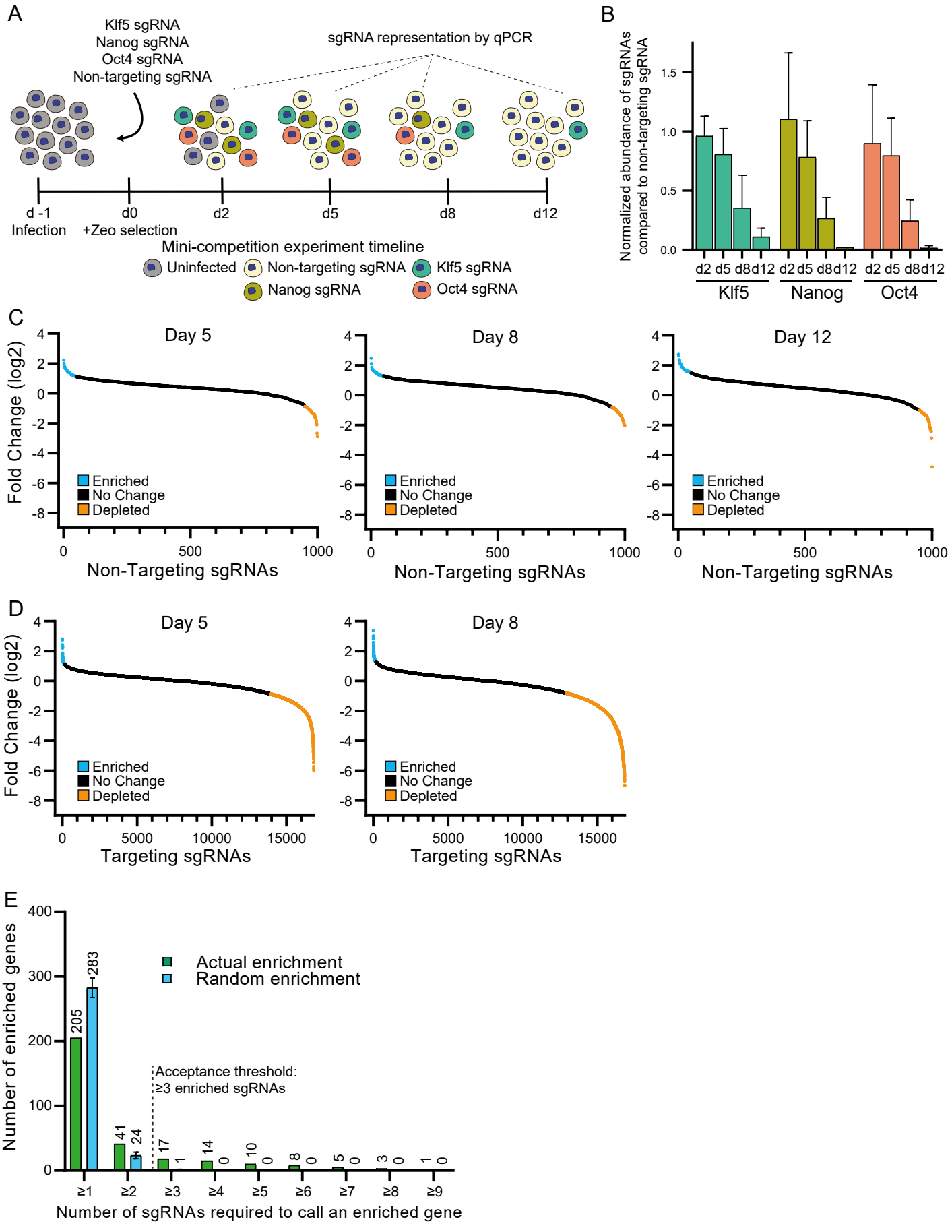
A
Klf5 sgRNA
Nanog sgRNA
Oct4 sgRNA
Non-targeting sgRNA
sgRNA representation by qPCR
d -1
Infection
d0
+Zeo selection
d2
d5
d8
d12
Mini-competition experiment timeline
Uninfected
Non-targeting sgRNA
Klf5 sgRNA
Nanog sgRNA
Oct4 sgRNA
B
Normalized abundance of sgRNAs compared to non-targeting sgRNA
d2 d5 d8 d12 d2 d5 d8 d12 d2 d5 d8 d12
Klf5
Nanog
Oct4
C
Day 5
Day 8
Day 12
Fold Change (log2)
Enriched
No Change
Depleted
Non-Targeting sgRNAs
D
Day 5
Day 8
Fold Change (log2)
Enriched
No Change
Depleted
Targeting sgRNAs
E
Number of enriched genes
Actual enrichment
Random enrichment
205
283
41
24
17
1
14
0
10
0
8
0
5
0
3
0
1
0
Acceptance threshold:
≥3 enriched sgRNAs
≥1
≥2
≥3
≥4
≥5
≥6
≥7
≥8
≥9
Number of sgRNAs required to call an enriched gene

Figure S2. Determination of candidate factors based on the false discovery rate (FDR) from non-targeting sgRNAs.

(A) Schematic overview of the qPCR competition assay to identify depletion dynamics. Representation of non-targeting and *Klf5*, *Oct4*, and *Nanog* targeting sgRNAs infected cells over 12 days of culture.

(B) Normalized abundance of *Klf5*, *Oct4*, *Nanog* targeting sgRNAs compared to non-targeting sgRNA with qPCR in collected samples for each time point (n=2). The abundance of pluripotency TFs is nullified within 12d.

(C) Log2 fold change of non-targeting sgRNAs on day 5, day 8, day 12 compared to the initial library representation. 50 most enriched sgRNAs are in blue and 50 most depleted sgRNAs are in orange. 50^{th} most enriched and 50^{th} most depleted sgRNAs were selected as the thresholds to call depleted and enriched targeting sgRNAs for each timepoint.

(D) Log2 fold change of targeting sgRNAs on day 5 and day 8 compared to the initial library representation. sgRNAs depleted more than the 50^{th} most depleted non-targeting sgRNA are in orange and enriched more than the 50^{th} most enriched non-targeting sgRNA are in blue.

(E) The number of actual sgRNAs enriched and mean sgRNAs number with random enrichment calculated by 1000 permutation tests with a different number of sgRNA per gene thresholds. TFs with more than or equal to 3 enriched sgRNAs are unlikely to be false positives.

Related to Figure 1.

Figure S3

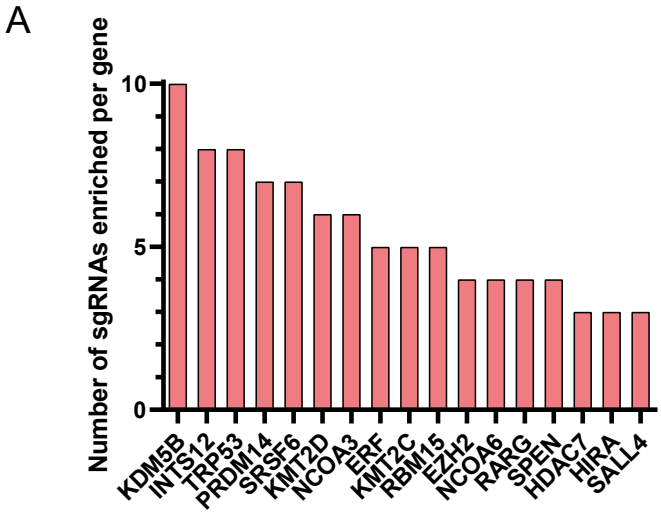
A
Number of sgRNAs enriched per gene
10
5
0
KDM5B
INTS12
TP53
PRDM14
SRSF6
KMT2D
NCOA3
ERF
KMT2C
RBM15
EZH2
NCOA6
RARG
SPEN
HDAC7
HIRA
SALL4

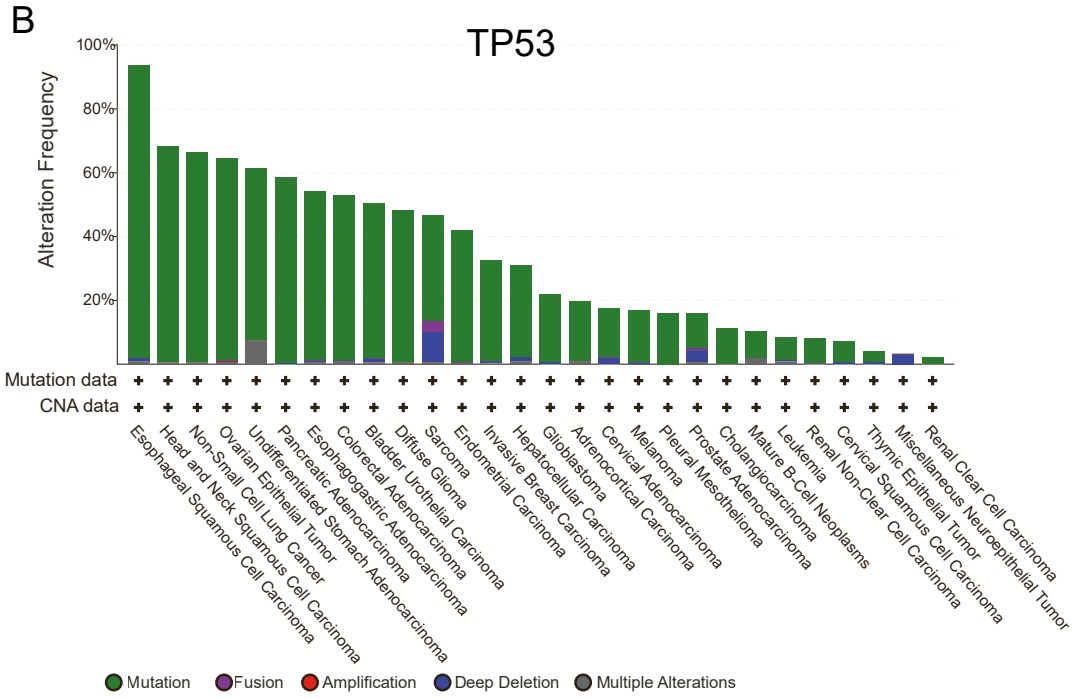
B
TP53
Alteration Frequency
100%
80%
60%
40%
20%
Mutation data
CNA data
Esophageal Squamous Cell Carcinoma
Head and Neck Squamous Cell Carcinoma
Non-Small Cell Lung Cancer
Ovarian Epithelial Tumor
Undifferentiated Stomach Adenocarcinoma
Pancreatic Adenocarcinoma
Esophagogastric Adenocarcinoma
Colorectal Adenocarcinoma
Bladder Urothelial Carcinoma
Diffuse Glioma
Sarcoma
Endometrial Carcinoma
Invasive Breast Carcinoma
Hepatocellular Carcinoma
Glioblastoma
Adrenocortical Carcinoma
Cervical Adenocarcinoma
Melanoma
Pleural Mesothelioma
Prostate Adenocarcinoma
Cholangiocarcinoma
Mature B-Cell Neoplasms
Leukemia
Renal Non-Clear Cell Carcinoma
Cervical Squamous Cell Carcinoma
Thymic Epithelial Tumor
Miscellaneous Neuroepithelial Tumor
Renal Clear Cell Carcinoma
Mutation
Fusion
Amplification
Deep Deletion
Multiple Alterations

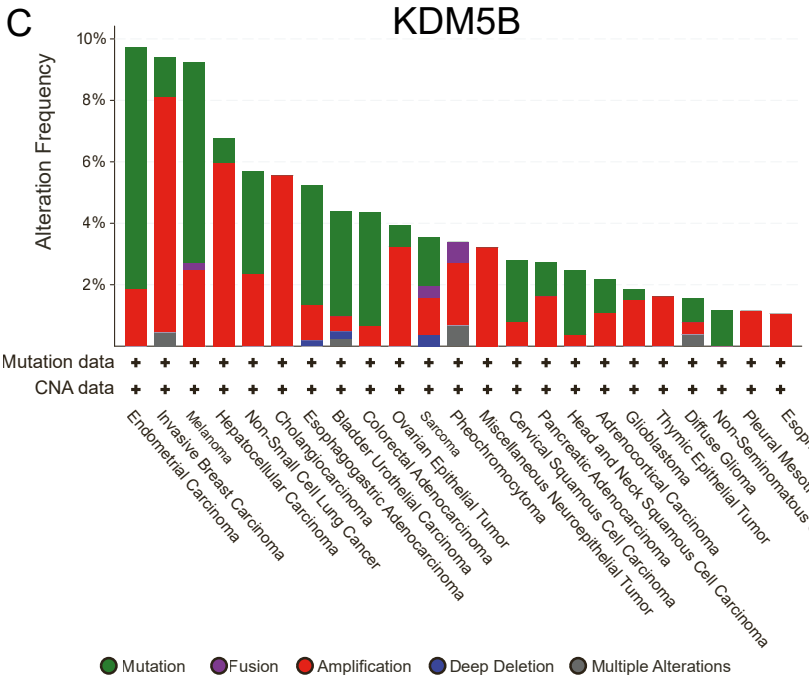
C
KDM5B
Alteration Frequency
10%
8%
6%
4%
2%
Mutation data
CNA data
Endometrial Carcinoma
Invasive Breast Carcinoma
Melanoma
Hepatocellular Carcinoma
Non-Small Cell Lung Cancer
Cholangiocarcinoma
Esophagogastric Adenocarcinoma
Bladder Urothelial Carcinoma
Colorectal Adenocarcinoma
Ovarian Epithelial Tumor
Sarcoma
Pheochromocytoma
Miscellaneous Neuroepithelial Tumor
Cervical Squamous Cell Carcinoma
Pancreatic Adenocarcinoma
Head and Neck Squamous Cell Carcinoma
Adrenocortical Carcinoma
Glioblastoma
Thymic Epithelial Tumor
Diffuse Glioma
Non-Seminomatous Germ Cell Tumor
Pleural Mesothelioma
Esophageal Squamous Cell Carcinoma
Mutation
Fusion
Amplification
Deep Deletion
Multiple Alterations

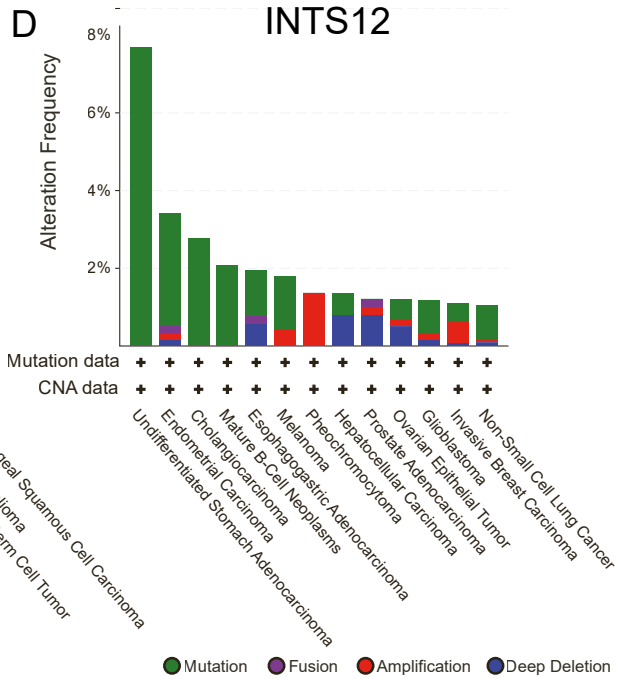
D
INTS12
Alteration Frequency
8%
6%
4%
2%
Mutation data
CNA data
Undifferentiated Stomach Adenocarcinoma
Endometrial Carcinoma
Cholangiocarcinoma
Mature B-Cell Neoplasms
Esophagogastric Adenocarcinoma
Melanoma
Pheochromocytoma
Hepatocellular Carcinoma
Prostate Adenocarcinoma
Ovarian Epithelial Tumor
Glioblastoma
Invasive Breast Carcinoma
Non-Small Cell Lung Cancer
Mutation
Fusion
Amplification
Deep Deletion

Figure S3. Enriched genes are mutated in cancers.

(A) 17 genes have 3 or more sgRNAs enriched on day 12.

(B) *Tp53*, **(C)** *Kdm2b*, **(D)** *Ints12* mutations incidence in various types of cancers (51799 patients). Data obtained from cBioPortal for Cancer Genomics. Enriched sgRNAs are targeting genes that are growth limiting, which are also found in cancer types.

Related to Figure 1.

Figure S4

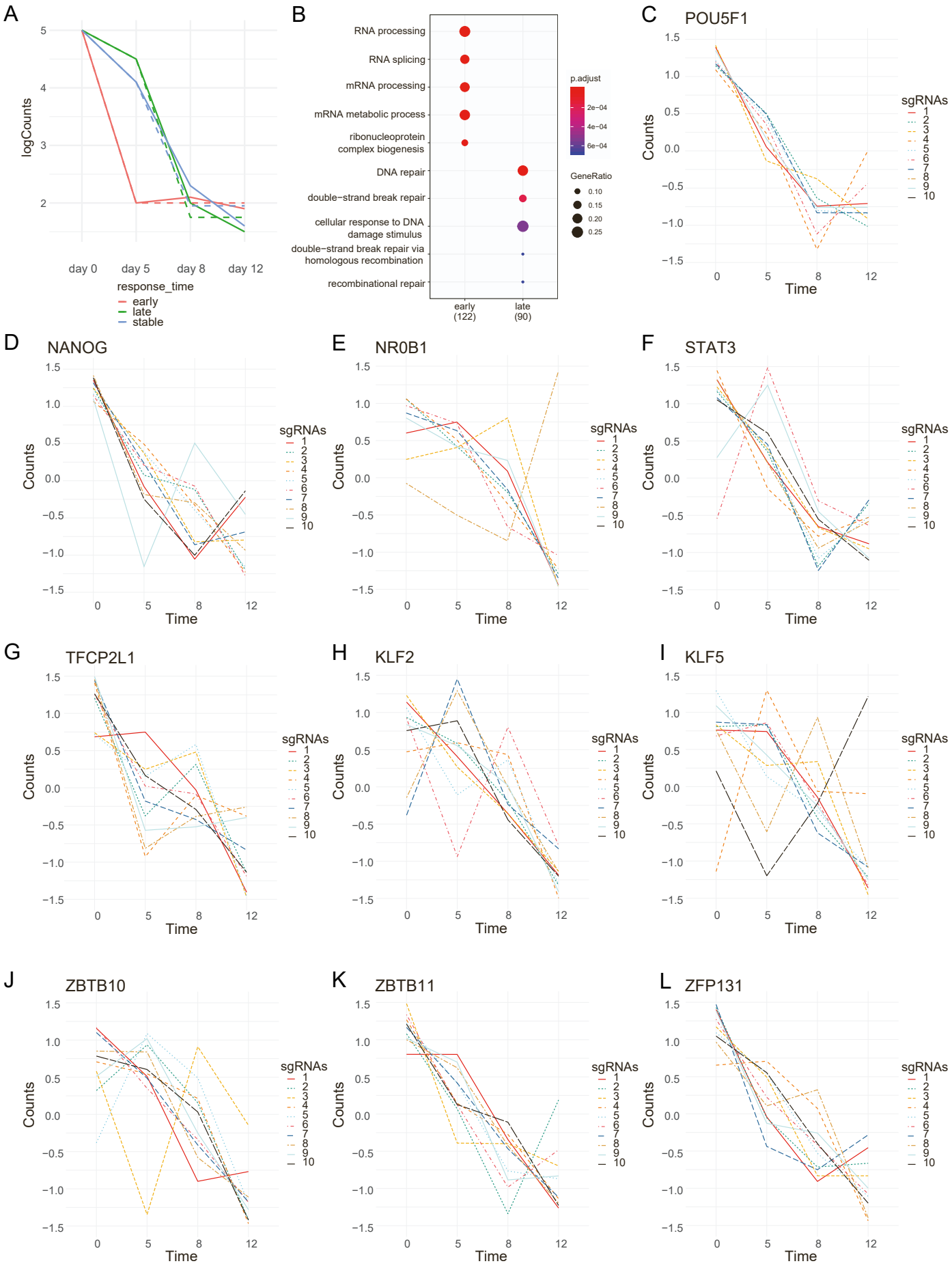
A
logCounts
day 0
day 5
day 8
day 12
response_time
early
late
stable
B
RNA processing
RNA splicing
mRNA processing
mRNA metabolic process
ribonucleoprotein complex biogenesis
DNA repair
double−strand break repair
cellular response to DNA damage stimulus
double−strand break repair via homologous recombination
recombinational repair
early (122)
late (90)
p.adjust
GeneRatio
C
POU5F1
D
NANOG
E
NR0B1
F
STAT3
G
TFCP2L1
H
KLF2
I
KLF5
J
ZBTB10
K
ZBTB11
L
ZFP131
Counts
Time
sgRNAs

Figure S4. Determination of candidate factors using a linear modeling method.

(A) Linear modeling for differential depletion categories of genes based on normalized sgRNA log counts. Three categories: early, stable, and late depleting were identified. The solid line is how the linear modeling is predicted and the dashed line is how the data fit to the projection.

(B) GO-enrichment analysis of early (n=122) and late (n=90) depleting factors throughout the screen. Gene Ratio is calculated with the number of occurrences in specific GO categories divided by the total amount of depleted TFs per category. Early category contains genes that are in core transcription machinery whereas late category contains genes that are playing roles in DNA damage.

(C) Linear regression of 10 sgRNAs targeting known core pluripotency factors *Oct4*, **(D)** *Nanog*, accessory factors (**(E)** *Nr0b1*, **(F)** *Stat3*, **(G)** *Tfcp2l1*), redundant accessory factors (**(H)** *Klf2*, **(I)** *Klf5*) and candidate hits from the screen (**(J)** *Zbtb10*, **(K)** *Zbtb11*, **(L)** *Zfp131*). *Oct4*, *Nanog*, *Zbtb11*, and *Zfp131* are in the early depleting category whereas accessory factors and *Zbtb10* are in the stable and the late depleting categories.

Related to Figure 1.

Figure S5

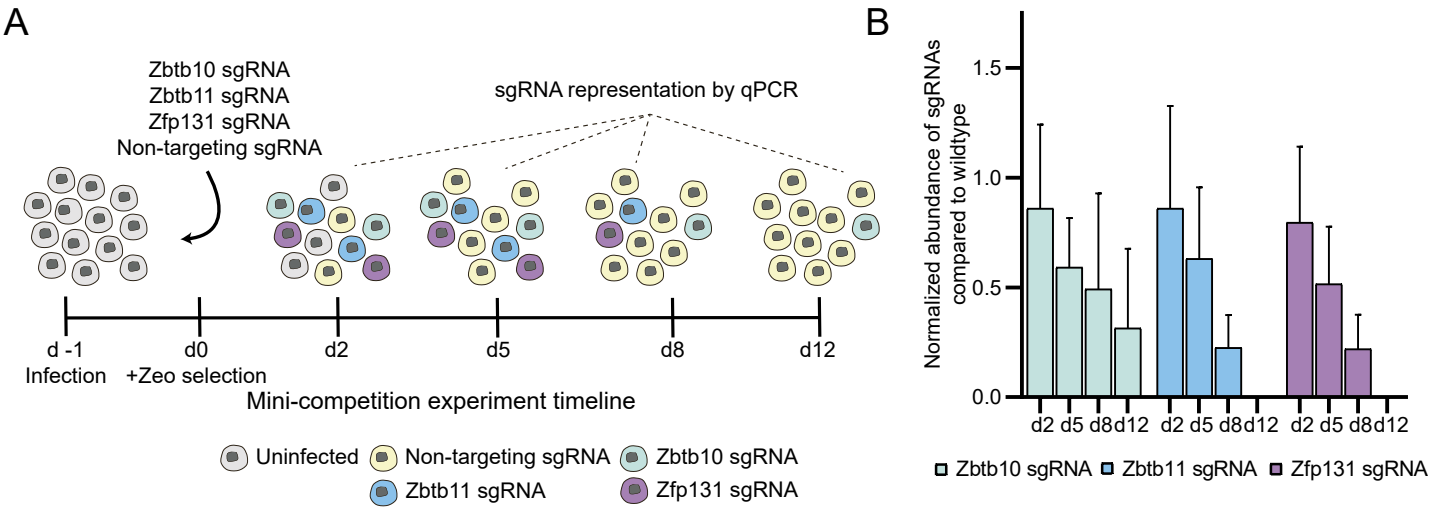
A
Zbtb10 sgRNA
Zbtb11 sgRNA
Zfp131 sgRNA
Non-targeting sgRNA
sgRNA representation by qPCR
d -1
Infection
d0
+Zeo selection
d2
d5
d8
d12
Mini-competition experiment timeline
Uninfected
Non-targeting sgRNA
Zbtb10 sgRNA
Zbtb11 sgRNA
Zfp131 sgRNA
B
Normalized abundance of sgRNAs compared to wildtype
1.5
1.0
0.5
0.0
d2 d5 d8 d12 d2 d5 d8 d12 d2 d5 d8 d12
Zbtb10 sgRNA
Zbtb11 sgRNA
Zfp131 sgRNA

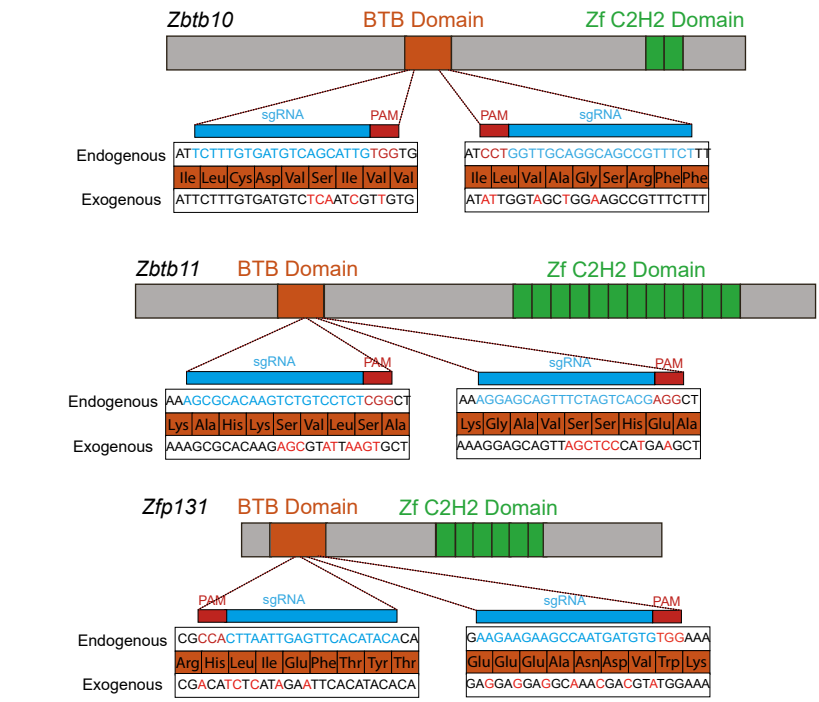
C
Zbtb10
BTB Domain
Zf C2H2 Domain
sgRNA
PAM
Endogenous
Exogenous
Zbtb11
Zfp131

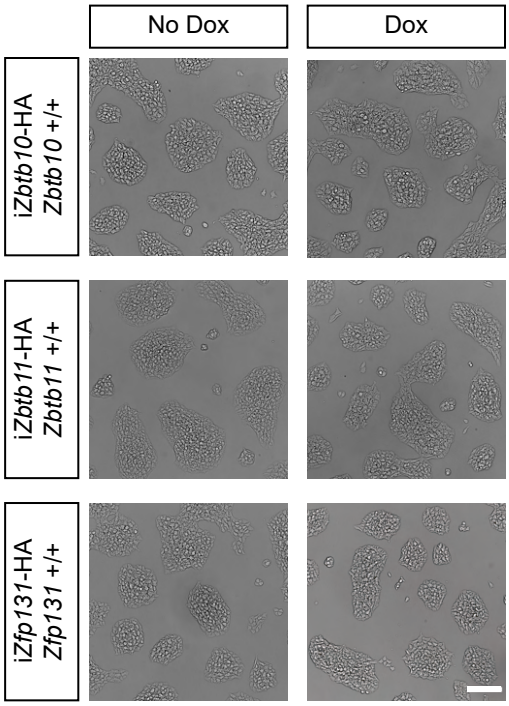
D
No Dox
Dox
iZbtb10-HA Zbtb10 +/+
iZbtb11-HA Zbtb11 +/+
iZfp131-HA Zfp131 +/+

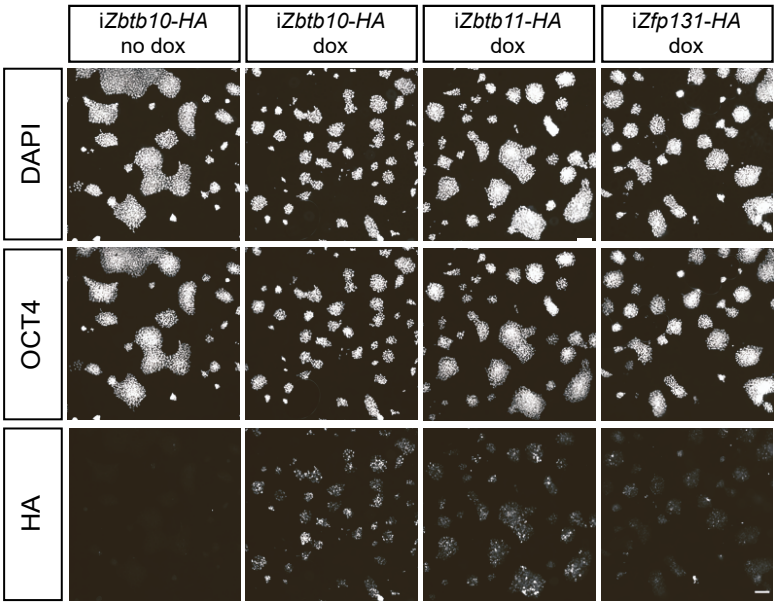
E
iZbtb10-HA no dox
iZbtb10-HA dox
iZbtb11-HA dox
iZfp131-HA dox
DAPI
OCT4
HA

Figure S5. Generation of conditional *Zbtb10Δ*, *Zbtb11Δ*, and *Zfp131Δ* lines

(A) Schematic overview of the TF candidate qPCR competition assay. Non-targeting and *Zbtb10*, *Zbtb11*, and *Zfp131* targeting sgRNAs infected cells representation over 12 days of culture.

(B) Normalized abundance of targeting sgRNAs compared to non-targeting sgRNA measured by qPCR in the competition experiment (n=2). *Zbtb10*, *Zbtb11*, and *Zfp131* targeting sgRNAs deplete compared to non-targeting one recapitulating the TF screen depletion dynamics.

(C) *Zbtb10*, *Zbtb11* and *Zfp131* genes illustrated with coding regions for interdomain linker regions (gray), BTB domain (orange) and C2H2 Zinc Finger domain (green). Two sgRNAs (blue sequences) targeting PAM sites (red sequences) at the endogenous BTB domain. HA-tagged exogenous copy of ZBTB10, ZBTB11, and ZFP131 expressed at the HPRT site contain silent mutations that disable the sgRNA binding and Cas9 cutting.

(D) Inducible *Zbtb10-HA*, *Zbtb11-HA* and *Zfp131-HA* lines with 48 h expression of exogenous alleles. Inducing transgenes do not cause any distinct morphological changes in ESCs. Scale bar = 200 μm.

(E) Oct4 and HA staining of inducible *Zbtb10-HA*, *Zbtb11-HA* and *Zfp131-HA* lines with 48h expression of exogenous alleles. Inducing transgenes do not alter *Oct4* expression in ESCs. Scale bar = 100 μm.

Related to Figure 1.

Figure S6

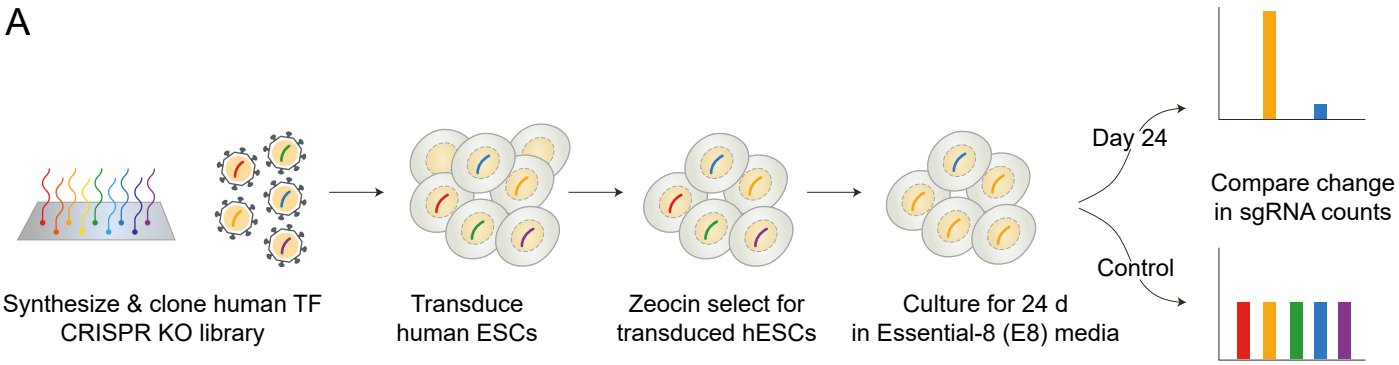
A
Day 24
Control
Compare change in sgRNA counts
Synthesize & clone human TF CRISPR KO library
Transduce human ESCs
Zeocin select for transduced hESCs
Culture for 24 d in Essential-8 (E8) media

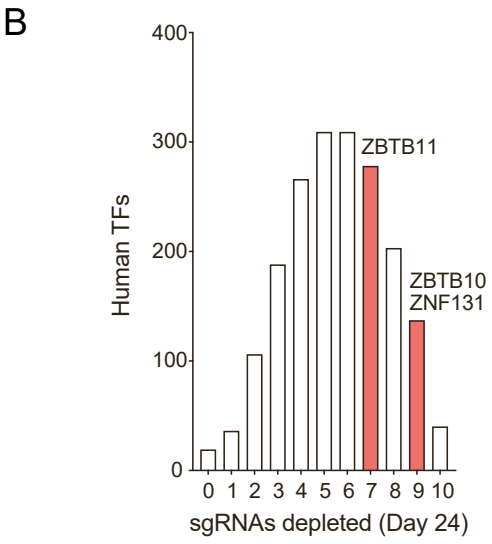
B
Human TFs
sgRNAs depleted (Day 24)
ZBTB11
ZBTB10
ZNF131

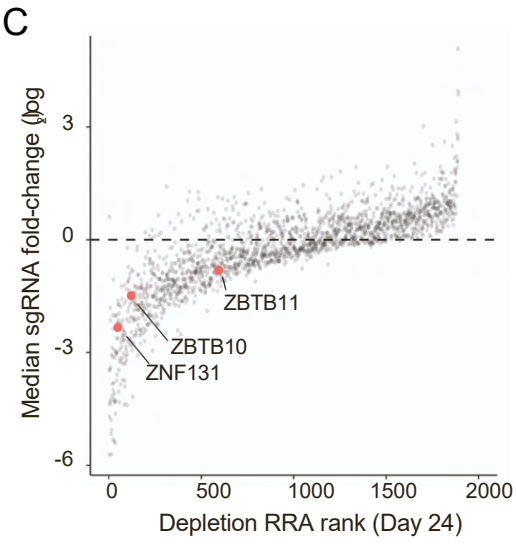
C
Median sgRNA fold-change (log2)
Depletion RRA rank (Day 24)
ZBTB11
ZBTB10
ZNF131

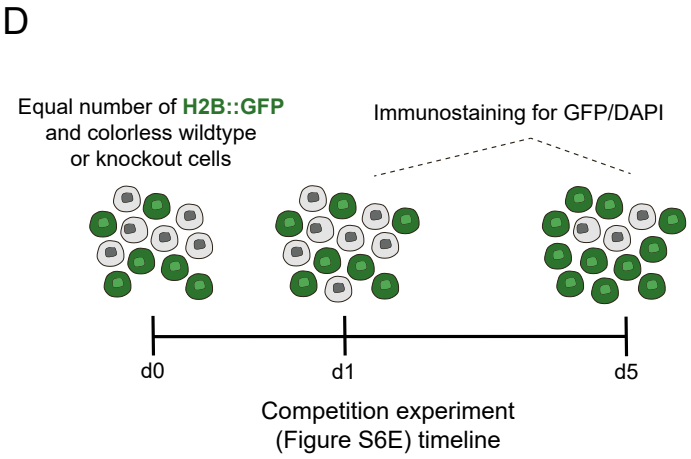
D
Equal number of H2B::GFP and colorless wildtype or knockout cells
Immunostaining for GFP/DAPI
d0
d1
d5
Competition experiment (Figure S6E) timeline

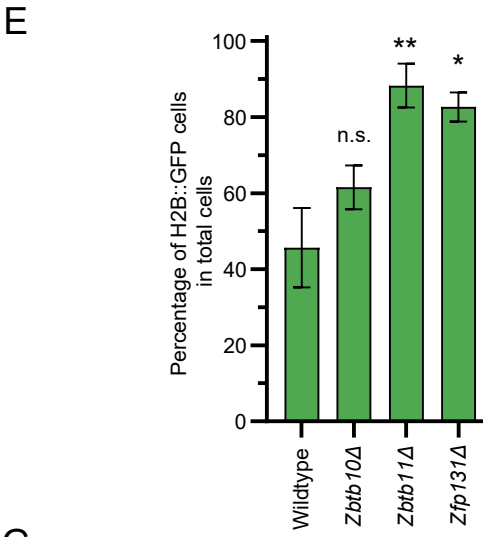
E
Percentage of H2B::GFP cells in total cells
n.s.
Wildtype
Zbtb10Δ
Zbtb11Δ
Zfp131Δ

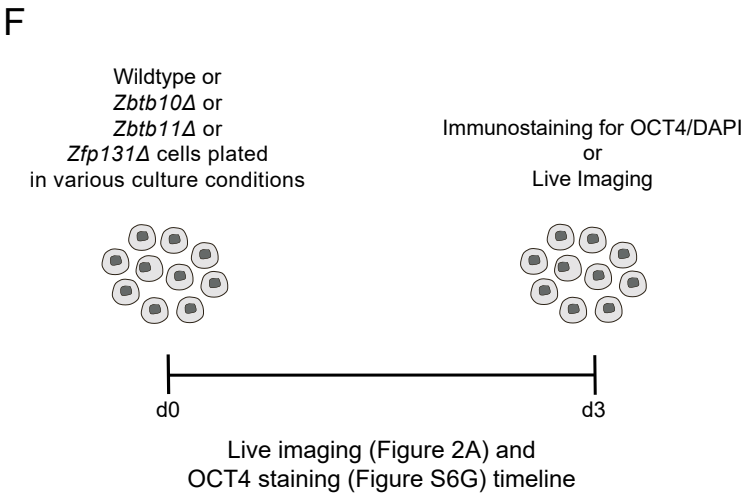
F
Wildtype or Zbtb10Δ or Zbtb11Δ or Zfp131Δ cells plated in various culture conditions
Immunostaining for OCT4/DAPI or Live Imaging
d0
d3
Live imaging (Figure 2A) and OCT4 staining (Figure S6G) timeline

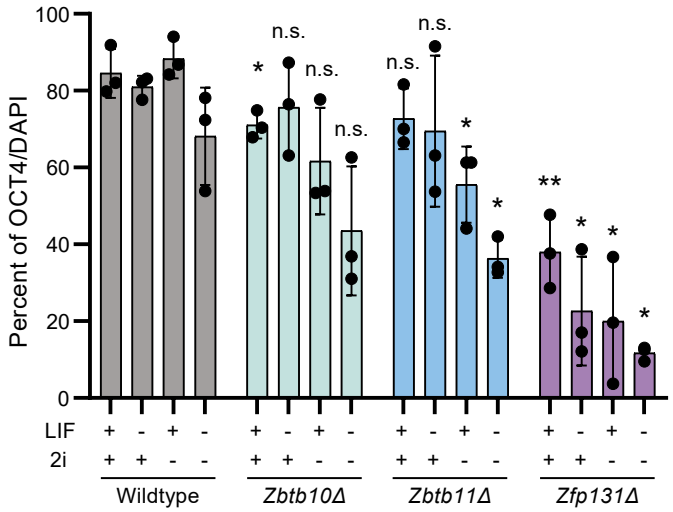
G
Percent of OCT4/DAPI
LIF
2i
Wildtype
Zbtb10Δ
Zbtb11Δ
Zfp131Δ

Figure S6. Human embryonic stem cell CRISPR loss-of-function screen identifies ZBTB10, ZBTB11, and ZNF131 as depleting genes.

(A) Schematic of human embryonic stem cell screen for TFs.

(B) Number of depleted sgRNAs for each TF using FDR < 0.05 threshold, as calculated from the non-targeting sgRNAs. ZBTB11 has 7 depleted sgRNAs, whereas ZBTB10 and ZNF131 have 9 depleted sgRNAs in hESCs.

(C) Median sgRNAs fold-change (log2) at day 24 as a function of RRA gene rank. sgRNAs targeting ZBTB10, ZBTB11 and ZFP131 have lower median rank denoting their role in hESCs.

(D) Schematic overview of the cell-growth competition assay. Clonal knockout *Zbtb10Δ*, *Zbtb11Δ,* and *Zfp131Δ* cells compete with GFP-labeled wt mouse ESCs.

(E) Percentage of non-GFP cells over time in cell growth competition assay of wt, *Zbtb10Δ*, *Zbtb11Δ,* and *Zfp131Δ* cells versus *H2b*::*Gfp* (n=3). Statistical analysis was performed by student's t-test, *p<0.05, **p<0.005. Mirroring pooled mutant analysis, wt ESCs readily outcompete *Zbtb11Δ* and *Zfp131Δ* cells.

(F) Schematic overview of the timeline for live imaging and immunostating experiments.

(G) OCT4/DAPI staining for wildtype, *Zbtb10Δ*, *Zbtb11Δ* and *Zfp131Δ* cells in 2i and LIF combination conditions (n=3). Statistical analysis was performed by student's t-test, *p<0.05, **p<0.005. *Zbtb11Δ* and *Zfp131Δ* cells have decreased OCT4 signal in specific culture conditions.

Related to Figure 1 and 2.

Figure S7

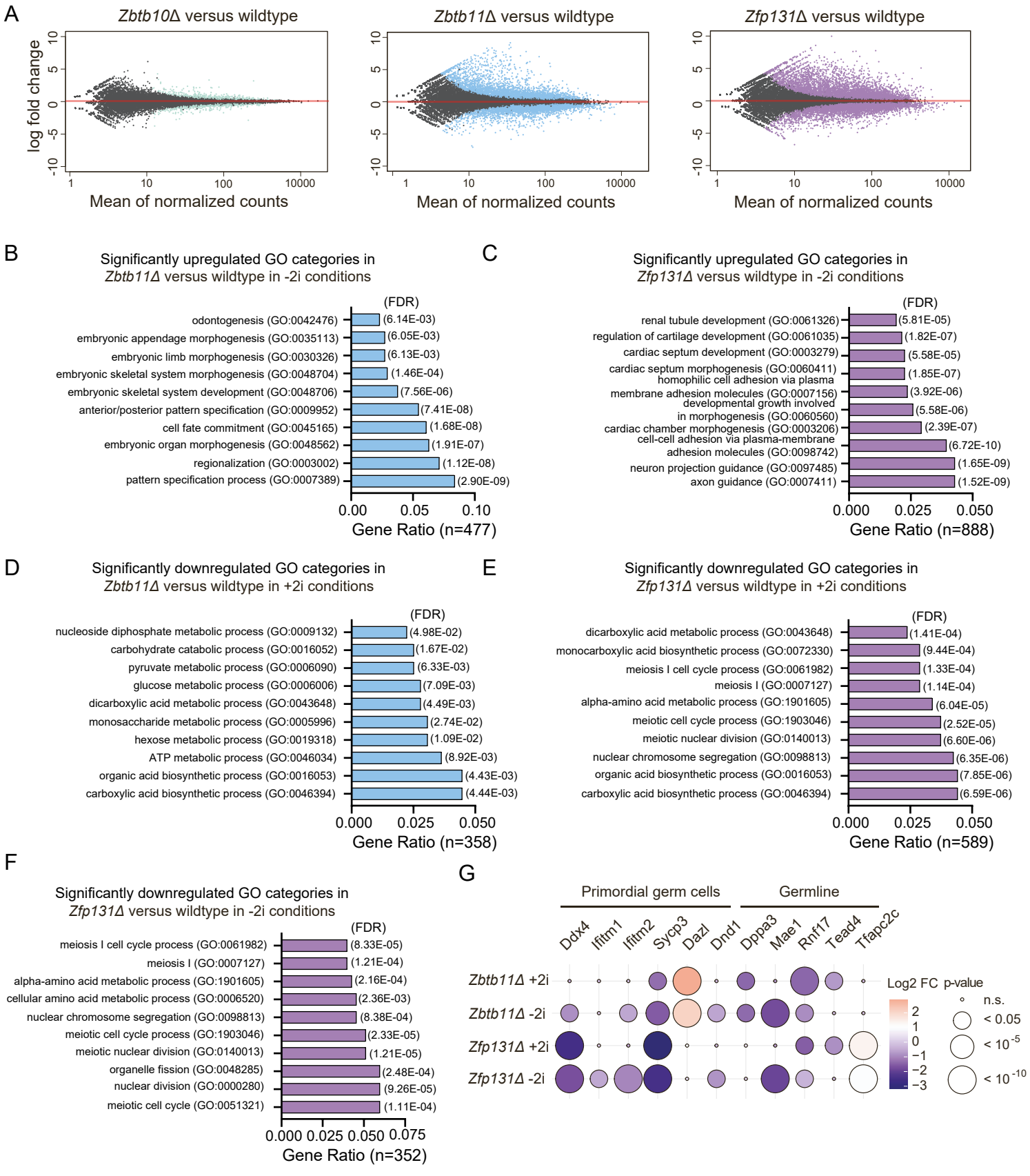
A
Zbtb10Δ versus wildtype
Zbtb11Δ versus wildtype
Zfp131Δ versus wildtype
log fold change
Mean of normalized counts
B
Significantly upregulated GO categories in Zbtb11Δ versus wildtype in -2i conditions
(FDR)
odontogenesis (GO:0042476) (6.14E-03)
embryonic appendage morphogenesis (GO:0035113) (6.05E-03)
embryonic limb morphogenesis (GO:0030326) (6.13E-03)
embryonic skeletal system morphogenesis (GO:0048704) (1.46E-04)
embryonic skeletal system development (GO:0048706) (7.56E-06)
anterior/posterior pattern specification (GO:0009952) (7.41E-08)
cell fate commitment (GO:0045165) (1.68E-08)
embryonic organ morphogenesis (GO:0048562) (1.91E-07)
regionalization (GO:0003002) (1.12E-08)
pattern specification process (GO:0007389) (2.90E-09)
Gene Ratio (n=477)
C
Significantly upregulated GO categories in Zfp131Δ versus wildtype in -2i conditions
(FDR)
renal tubule development (GO:0061326) (5.81E-05)
regulation of cartilage development (GO:0061035) (1.82E-07)
cardiac septum development (GO:0003279) (5.58E-05)
cardiac septum morphogenesis (GO:0060411) (1.85E-07)
homophilic cell adhesion via plasma membrane adhesion molecules (GO:0007156) (3.92E-06)
developmental growth involved in morphogenesis (GO:0060560) (5.58E-06)
cardiac chamber morphogenesis (GO:0003206) (2.39E-07)
cell-cell adhesion via plasma-membrane adhesion molecules (GO:0098742) (6.72E-10)
neuron projection guidance (GO:0097485) (1.65E-09)
axon guidance (GO:0007411) (1.52E-09)
Gene Ratio (n=888)
D
Significantly downregulated GO categories in Zbtb11Δ versus wildtype in +2i conditions
(FDR)
nucleoside diphosphate metabolic process (GO:0009132) (4.98E-02)
carbohydrate catabolic process (GO:0016052) (1.67E-02)
pyruvate metabolic process (GO:0006090) (6.33E-03)
glucose metabolic process (GO:0006006) (7.09E-03)
dicarboxylic acid metabolic process (GO:0043648) (4.49E-03)
monosaccharide metabolic process (GO:0005996) (2.74E-02)
hexose metabolic process (GO:0019318) (1.09E-02)
ATP metabolic process (GO:0046034) (8.92E-03)
organic acid biosynthetic process (GO:0016053) (4.43E-03)
carboxylic acid biosynthetic process (GO:0046394) (4.44E-03)
Gene Ratio (n=358)
E
Significantly downregulated GO categories in Zfp131Δ versus wildtype in +2i conditions
(FDR)
dicarboxylic acid metabolic process (GO:0043648) (1.41E-04)
monocarboxylic acid biosynthetic process (GO:0072330) (9.44E-04)
meiosis I cell cycle process (GO:0061982) (1.33E-04)
meiosis I (GO:0007127) (1.14E-04)
alpha-amino acid metabolic process (GO:1901605) (6.04E-05)
meiotic cell cycle process (GO:1903046) (2.52E-05)
meiotic nuclear division (GO:0140013) (6.60E-06)
nuclear chromosome segregation (GO:0098813) (6.35E-06)
organic acid biosynthetic process (GO:0016053) (7.85E-06)
carboxylic acid biosynthetic process (GO:0046394) (6.59E-06)
Gene Ratio (n=589)
F
Significantly downregulated GO categories in Zfp131Δ versus wildtype in -2i conditions
(FDR)
meiosis I cell cycle process (GO:0061982) (8.33E-05)
meiosis I (GO:0007127) (1.21E-04)
alpha-amino acid metabolic process (GO:1901605) (2.16E-04)
cellular amino acid metabolic process (GO:0006520) (2.36E-03)
nuclear chromosome segregation (GO:0098813) (8.38E-04)
meiotic cell cycle process (GO:1903046) (2.33E-05)
meiotic nuclear division (GO:0140013) (1.21E-05)
organelle fission (GO:0048285) (2.48E-04)
nuclear division (GO:0000280) (9.26E-05)
meiotic cell cycle (GO:0051321) (1.11E-04)
Gene Ratio (n=352)
G
Primordial germ cells
Germline
Ddx4
Ifitm1
Ifitm2
Sycp3
Dazl
Dnd1
Dppa3
Mae1
Rnf17
Tead4
Tfapc2c
Zbtb11Δ +2i
Zbtb11Δ -2i
Zfp131Δ +2i
Zfp131Δ -2i
Log2 FC
p-value
n.s.
< 0.05
< 10-5
< 10-10

Figure S7. *Zbtb11Δ* and *Zfp131Δ* knockout cells express multiple lineage-specific markers in -2i conditions.

(A) Volcano plots of log2 fold change of transcripts expressed in *Zbtb10Δ*, *Zbtb11Δ* and *Zfp131Δ* cells versus wt cells grown in the absence of doxycycline for 3d in -2i+LIF media (n=3). Significant changes (* $p<0.05$) marked in color for each genotype. *Zbtb11* and *Zfp131* mutations induce aberrant gene expression.

(B) GO-enrichment analysis of significantly upregulated genes in *Zbtb11Δ* in -2i condition (n=477), **(C)** significantly upregulated genes in *Zfp131Δ* in -2i condition (n=888), **(D)** significantly downregulated genes in *Zbtb11Δ* in +2i condition (n=358), **(E)** significantly downregulated genes in *Zfp131Δ* in +2i condition (n=589), and **(F)** significantly downregulated genes in *Zfp131Δ* in -2i condition (n=352). Gene Ratio is calculated with the number of occurrences in specific GO categories divided by the total amount of genes. The low number of downregulated genes in -2i conditions for *Zbtb11Δ* produced no significant GO-term enriched.

(G) The log2 fold change of TFs obtained from bulk RNAseq experiment in *Zbtb11Δ* and *Zfp131Δ* cells versus wildtype in plus and minus 2i conditions. (n.s. Not significant) (n=3). No aberrant expression of primordial germ cells and germline TFs detected in *Zbtb11Δ* and *Zfp131Δ* cells.

Related to Figure 2.

Figure S8

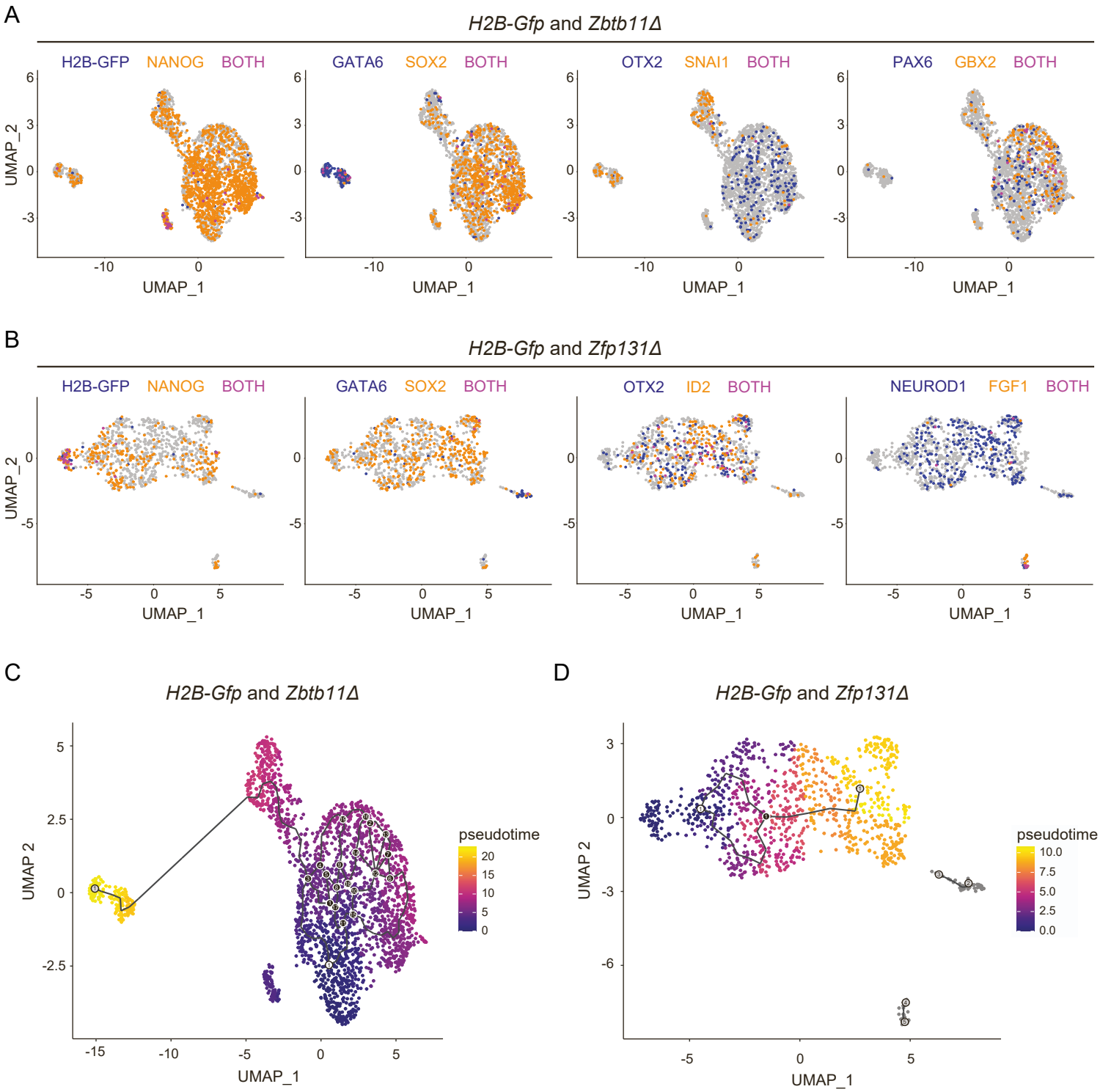
A
H2B-Gfp and Zbtb11Δ
H2B-GFP NANOG BOTH
GATA6 SOX2 BOTH
OTX2 SNAI1 BOTH
PAX6 GBX2 BOTH
UMAP_2
UMAP_1
B
H2B-Gfp and Zfp131Δ
H2B-GFP NANOG BOTH
GATA6 SOX2 BOTH
OTX2 ID2 BOTH
NEUROD1 FGF1 BOTH
UMAP_2
UMAP_1
C
H2B-Gfp and Zbtb11Δ
UMAP 2
UMAP_1
pseudotime
20
15
10
5
0
D
H2B-Gfp and Zfp131Δ
UMAP 2
UMAP_1
pseudotime
10.0
7.5
5.0
2.5
0.0

Figure S8. *Zbtb11Δ* and *Zfp131Δ* knockout cells differentiate into multiple lineages.

(A) Expression of H2B-GFP and genes associated with pluripotency (NANOG, SOX2) and germ layers (GATA6, OTX2, SNAI, GBX2, PAX6, ID2, FGF1, NEUROD1) in *Zbtb11Δ* and H2B-Gfp cells, and **(B)** *Zfp131Δ* and *H2B-Gfp* cells. *Zbtb11* and *Zfp131* knockout cells segregate in different clusters compared to *H2b::Gfp* and express developmentally regulated genes.

(C) Differentiation trajectories of *Zbtb11Δ* and **(D)** *Zfp131Δ* using pseudotime analysis with Monocle3 algorithm. Black lines show the structure and trajectory of the graph. The white circle with the number 1 is the origin of differentiation. Light gray circles denote a different outcome (individual cell fates in this case). Every branching node is denoted with a black circle with numbers. Gray circles with numbers.

Related to Figure 3.

Figure S9

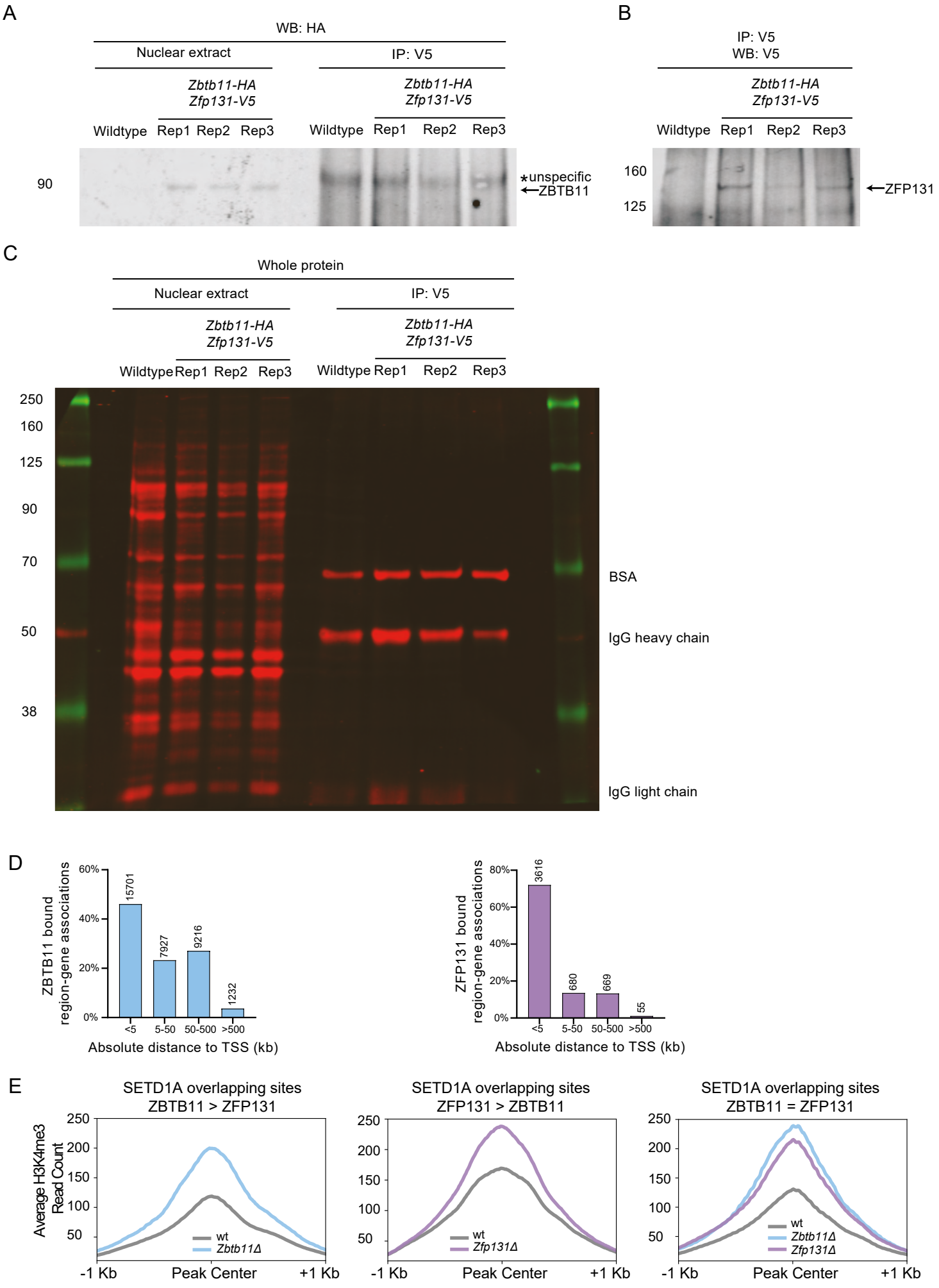
A
WB: HA
Nuclear extract
IP: V5
Zbtb11-HA
Zfp131-V5
Wildtype
Rep1
Rep2
Rep3
90
*unspecific
ZBTB11
B
IP: V5
WB: V5
160
125
ZFP131
C
Whole protein
250
160
125
90
70
50
38
BSA
IgG heavy chain
IgG light chain
D
ZBTB11 bound region-gene associations
60%
40%
20%
0%
15701
7927
9216
1232
<5
5-50
50-500
>500
Absolute distance to TSS (kb)
ZFP131 bound region-gene associations
80%
60%
40%
20%
0%
3616
680
669
55
Absolute distance to TSS (kb)
E
SETD1A overlapping sites
ZBTB11 > ZFP131
ZFP131 > ZBTB11
ZBTB11 = ZFP131
Average H3K4me3 Read Count
250
200
150
100
50
wt
Zbtb11Δ
Zfp131Δ
-1 Kb
Peak Center
+1 Kb

Figure S9. ZBTB11 and ZFP131 do not heterodimerize in ESCs, bind proximally to TSS and *Zbtb11* and *Zfp131* mutation leads to high H3K4me3 gain at SETD1A present sites

(A) Western blot for ZBTB11-HA in whole nuclear extract and V5 immunoprecipitated samples in *Zbtb11-HA Zfp131-V5* ESCs (n=3). Wildtype does not have any HA and V5 tags. Therefore, the band presenting in the IP V5 wildtype lane indicated nonspecific HA in all IP V5 samples. ZBTB11 and ZFP131 do not heterodimerize in ESCs.

(B) Western blot for ZFP131-V5 in V5 immunoprecipitated samples in *Zbtb11-HA Zfp131-V5* ESCs (n=3), showing the IP was successful.

(C) Whole protein staining of the membrane shown in panel A and B.

(D) The proximity of all ZBTB11 and ZFP131 bound regions to TSS based on GREAT algorithm. Both TFs bind proximal to TSSs.

(E) Metagene plots for H3K4me3 signal difference in ZBTB11 and SETD1A co-bound sites in *Zbtb11Δ* versus wt, in ZFP131 and SETD1A co-bound sites in *Zfp131Δ* versus wt, in ZBTB11, ZFP131 and SETD1A co-bound sites in all three lines (n=2 for all). ZBTB11 and ZFP131 removal induced H3K4me3 gain at SETD1A present sites in wt cells. H3K4me3 comparison was done on -2i+LIF condition.

Related to Figure 4.

Figure S10

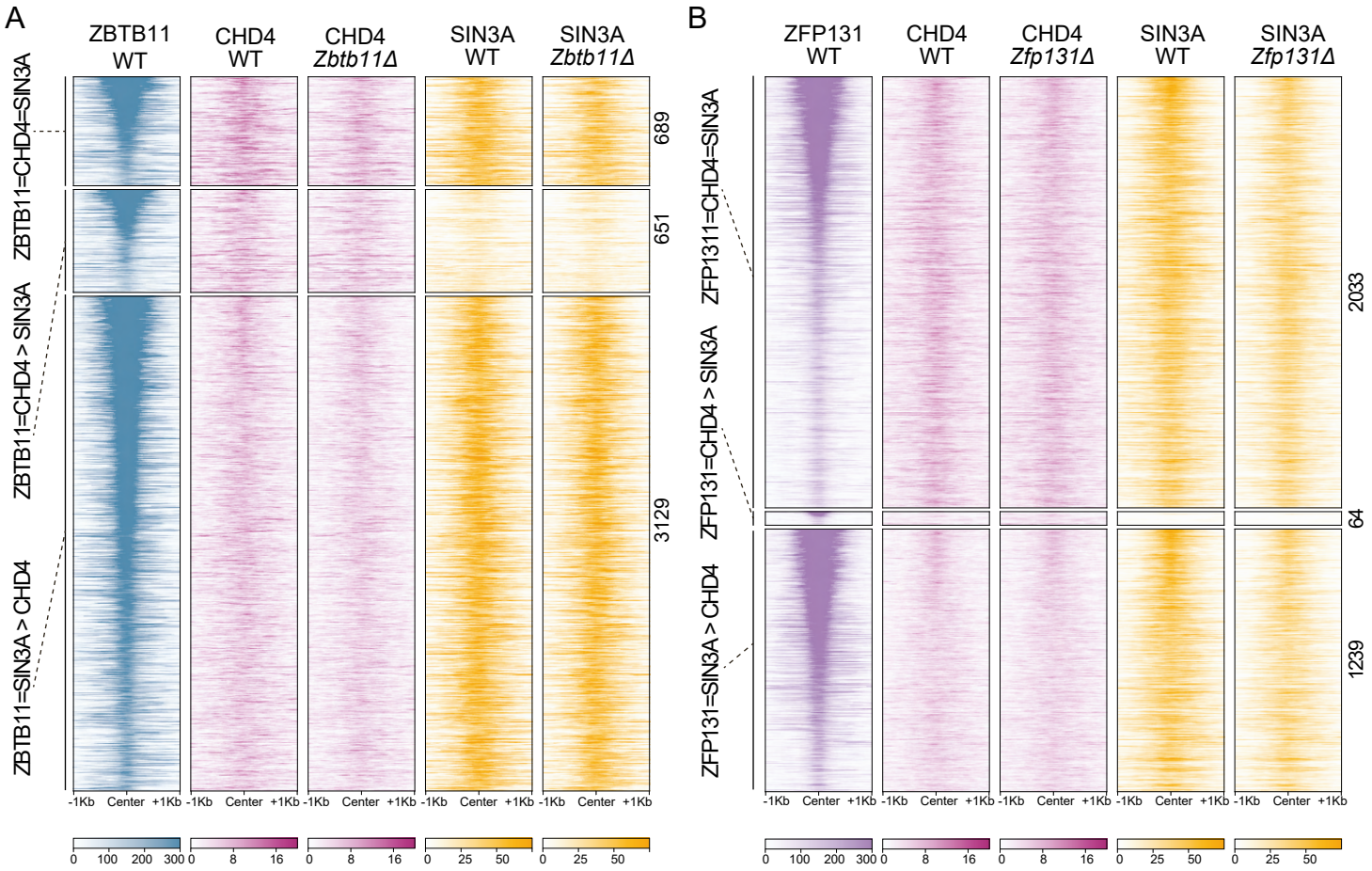
A
ZBTB11 WT
CHD4 WT
CHD4 Zbtb11Δ
SIN3A WT
SIN3A Zbtb11Δ
ZBTB11=CHD4=SIN3A
ZBTB11=CHD4 > SIN3A
ZBTB11=SIN3A > CHD4
689
651
3129
-1Kb Center +1Kb
0 100 200 300
0 8 16
0 25 50
B
ZFP131 WT
CHD4 WT
CHD4 Zfp131Δ
SIN3A WT
SIN3A Zfp131Δ
ZFP1311=CHD4=SIN3A
ZFP131=CHD4 > SIN3A
ZFP131=SIN3A > CHD4
2033
64
1239

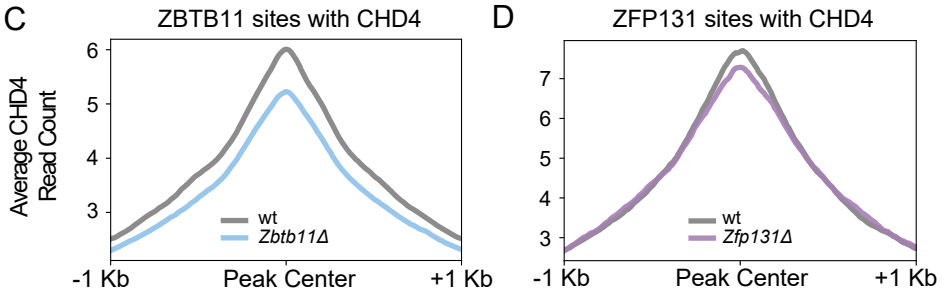
C
ZBTB11 sites with CHD4
Average CHD4 Read Count
wt
Zbtb11Δ
-1 Kb
Peak Center
+1 Kb
D
ZFP131 sites with CHD4
wt
Zfp131Δ

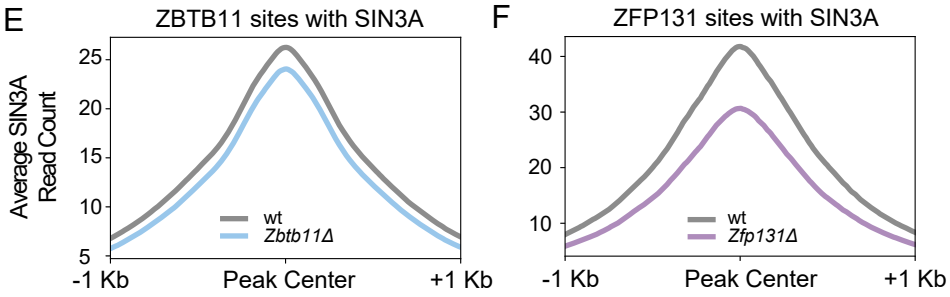
E
ZBTB11 sites with SIN3A
Average SIN3A Read Count
wt
Zbtb11Δ
-1 Kb
Peak Center
+1 Kb
F
ZFP131 sites with SIN3A
wt
Zfp131Δ

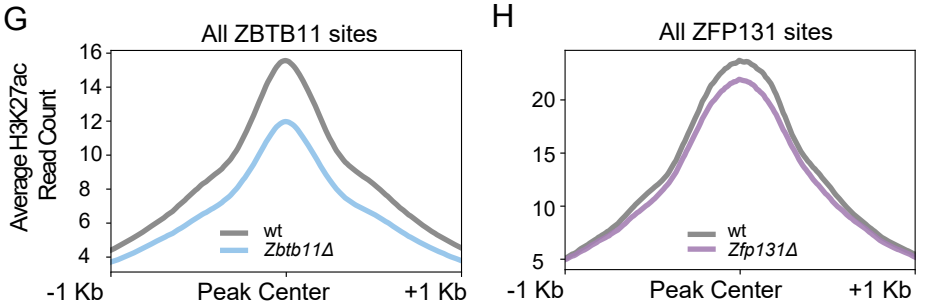
G
All ZBTB11 sites
Average H3K27ac Read Count
wt
Zbtb11Δ
-1 Kb
Peak Center
+1 Kb
H
All ZFP131 sites
wt
Zfp131Δ

Figure S10. ZBTB11 and ZFP131 cobound with CHD4 and SIN3A.

(A) ChIP-seq heatmap for ZBTB11 overlap with CHD4 and SIN3A in *Zbtb11Δ* and wt cells (n=2 for all).

(B) ChIP-seq heatmap for ZFP131 overlap with CHD4 and SIN3A in *Zfp131Δ* and wt cells (n=2 for all).

(C) Metagene plots for CHD4 binding difference in *Zbtb11Δ* versus wt (n=2) and in **(D)** *Zfp131Δ* versus wt (n=2).

(E) Metagene plots for SIN3A binding difference in *Zbtb11Δ* versus wt (n=2) and in **(F)** *Zfp131Δ* versus wt (n=2). Both knockouts have a slight decrease in CHD4 and SIN3A binding compared to wt.

(G) Metagene plots for H3K27ac at ZBTB11 bound sites in *Zbtb11Δ* and wt ESCs (n=2) and **(H)** at ZFP131 bound sites in *Zfp131Δ* versus wt (n=2). Both knockouts have a decrease in H3K27ac contrary to the expected increase. CHD4, SIN3A and H3K27ac comparison were done in -2i+LIF condition.

Related to Figure 4.

Figure S11

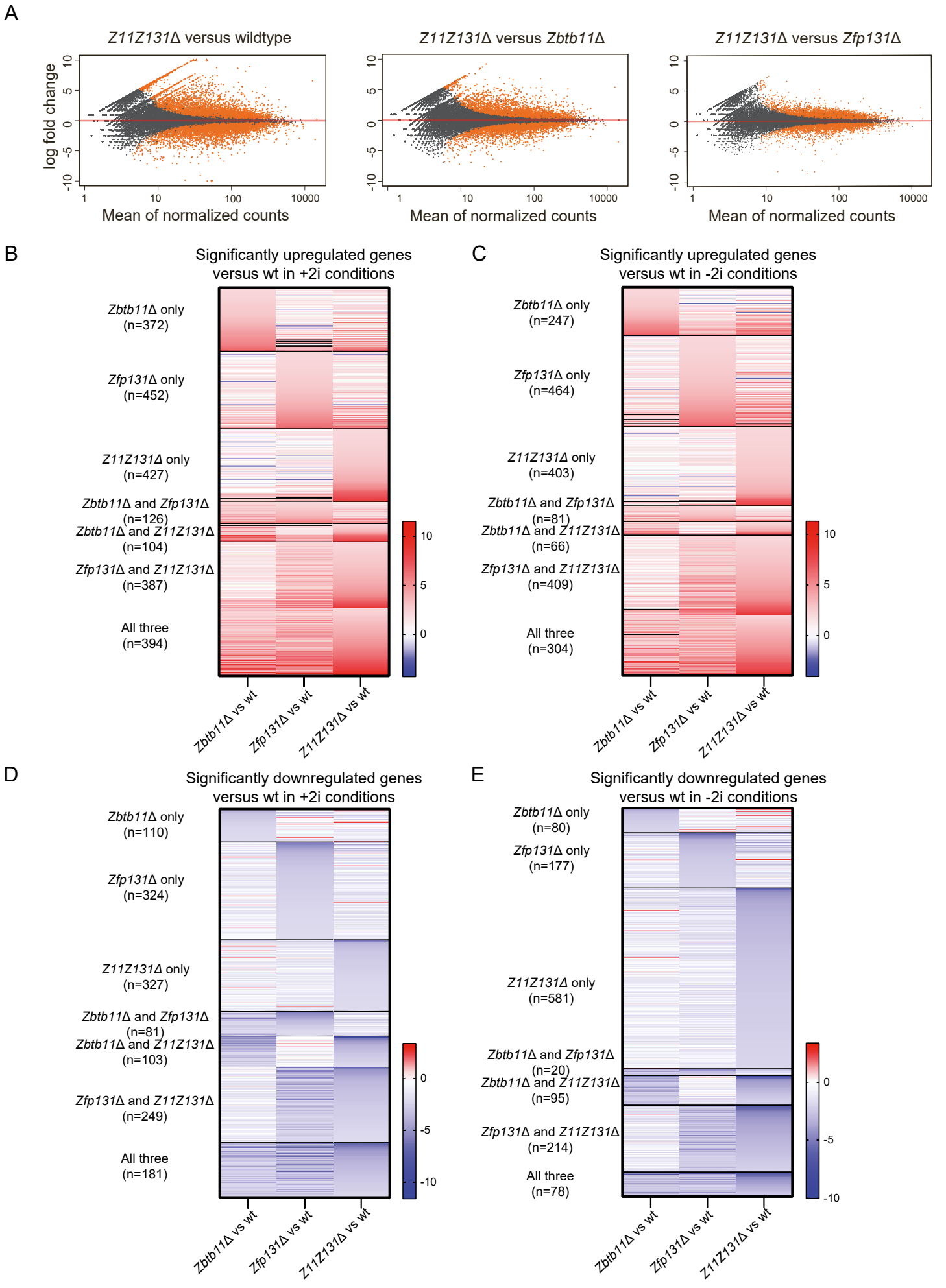
A
Z11Z131Δ versus wildtype
Z11Z131Δ versus Zbtb11Δ
Z11Z131Δ versus Zfp131Δ
log fold change
Mean of normalized counts
B
Significantly upregulated genes versus wt in +2i conditions
Zbtb11Δ only (n=372)
Zfp131Δ only (n=452)
Z11Z131Δ only (n=427)
Zbtb11Δ and Zfp131Δ (n=126)
Zbtb11Δ and Z11Z131Δ (n=104)
Zfp131Δ and Z11Z131Δ (n=387)
All three (n=394)
Zbtb11Δ vs wt
Zfp131Δ vs wt
Z11Z131Δ vs wt
C
Significantly upregulated genes versus wt in -2i conditions
Zbtb11Δ only (n=247)
Zfp131Δ only (n=464)
Z11Z131Δ only (n=403)
Zbtb11Δ and Zfp131Δ (n=81)
Zbtb11Δ and Z11Z131Δ (n=66)
Zfp131Δ and Z11Z131Δ (n=409)
All three (n=304)
D
Significantly downregulated genes versus wt in +2i conditions
Zbtb11Δ only (n=110)
Zfp131Δ only (n=324)
Z11Z131Δ only (n=327)
Zbtb11Δ and Zfp131Δ (n=81)
Zbtb11Δ and Z11Z131Δ (n=103)
Zfp131Δ and Z11Z131Δ (n=249)
All three (n=181)
E
Significantly downregulated genes versus wt in -2i conditions
Zbtb11Δ only (n=80)
Zfp131Δ only (n=177)
Z11Z131Δ only (n=581)
Zbtb11Δ and Zfp131Δ (n=20)
Zbtb11Δ and Z11Z131Δ (n=95)
Zfp131Δ and Z11Z131Δ (n=214)
All three (n=78)

Figure S11. Double knock-out is not an additive phenotype of both knock-outs, and single knock-out is not epistatic to the other.

(A) Volcano plots of log2 fold change of transcripts expressed in *Z11Z131Δ* cells versus wt, *Zbtb11*, and *Zbtb131Δ* cells grown in the absence of doxycycline for 3d in -2i+LIF media (n=3). Significant changes (* $p<0.05$) marked in orange.

(B) Significantly upregulated genes in *Zbtb11, Zbtb131Δ,* and *Z11Z131Δ* cells versus wt in +2i+LIF, **(C)** upregulated genes in -2i+LIF, **(D)** downregulated genes in +2i+LIF, and **(E)** downregulated genes in -2i+LIF (n=3 for all). Many genes are only upregulated in single or double knock-outs only, therefore knock-outs are not epistatic. Related to Figure 7.

Figure S12

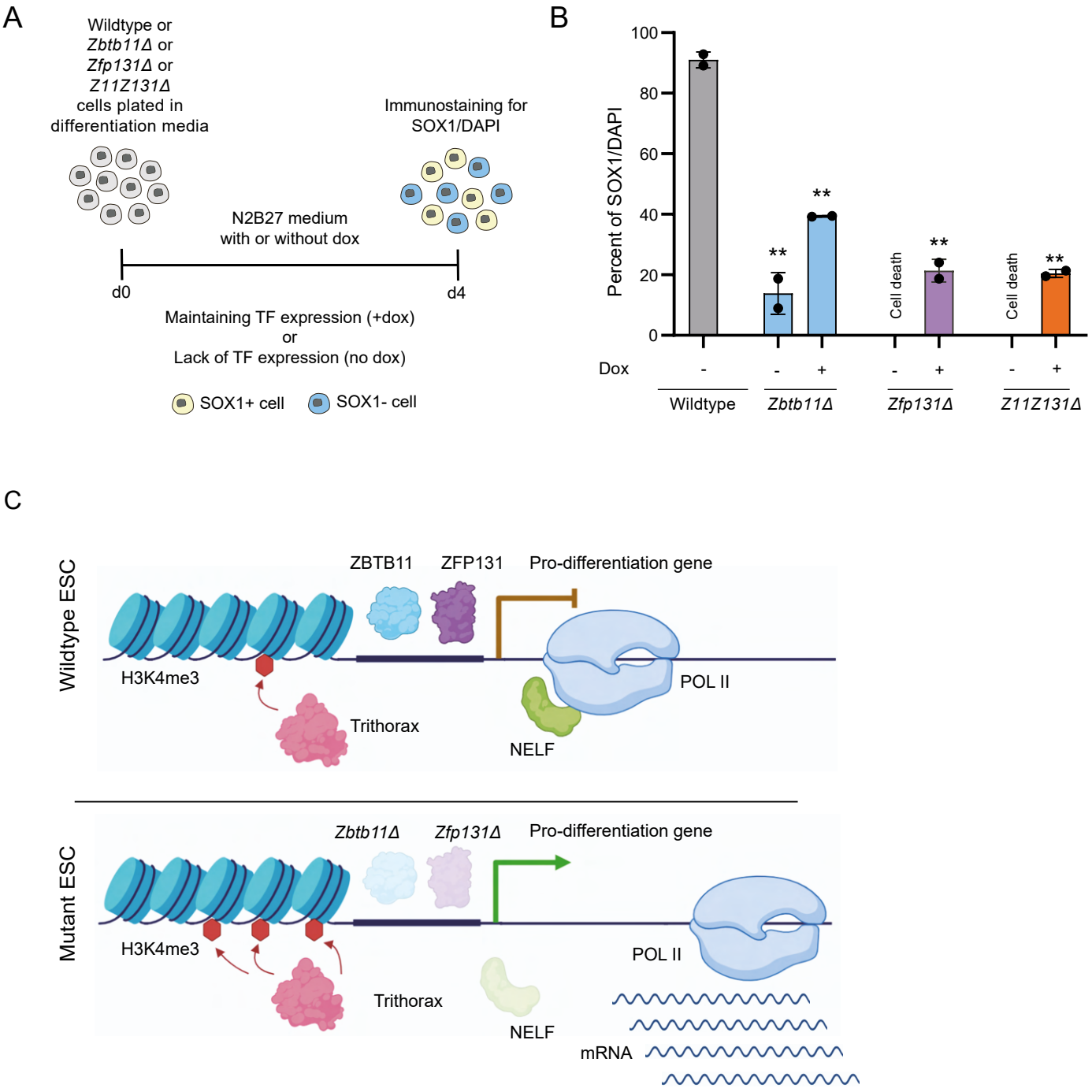
A
Wildtype or
Zbtb11Δ or
Zfp131Δ or
Z11Z131Δ
cells plated in
differentiation media
Immunostaining for
SOX1/DAPI
N2B27 medium
with or without dox
d0
d4
Maintaining TF expression (+dox)
or
Lack of TF expression (no dox)
SOX1+ cell
SOX1- cell
B
Percent of SOX1/DAPI
100
80
60
40
20
0
**
**
**
**
Cell death
Cell death
Dox
-
-
+
-
+
-
+
Wildtype
Zbtb11Δ
Zfp131Δ
Z11Z131Δ
C
Wildtype ESC
ZBTB11
ZFP131
Pro-differentiation gene
H3K4me3
Trithorax
POL II
NELF
Mutant ESC
Zbtb11Δ
Zfp131Δ
Pro-differentiation gene
H3K4me3
Trithorax
POL II
NELF
mRNA

Figure S12. Maintaining ZBTB TF expression preserves pluripotency and blocks differentiation.

(A) Schematic overview of NPC differentiation in the absence of ZBTB TFs or while forced expression of ZBTB TFs during differentiation.

(B) Differentiation efficiency calculated by SOX1+/DAPI in single and double knock-outs versus wt. Forced expression of single or both ZBTB TFs block differentiation efficiency. Lack of *Zbtb11Δ* reduces differentiation efficiency compared to wt. *Zbtb131Δ* and *Z11Z131Δ* cells did not survive in differentiation conditions (n=2). Statistical analysis was performed by student's t-test, n.s. Not significant, *p<0.05, **p<0.005.

(C) Schematic overview of the mode-of-action of ZBTB11 and ZFP131 in ESCs. ZBTB11 and ZFP131 bind proximal to pro-differentiation genes. These genes contain POL II and NELF, and active chromatin features. Upon ZBTB11 and ZFP131 removal, TrxG increases activity, and POL II transcribes pro-differentiation genes causing ESC to differentiate and exit their pluripotent state.

Related to Figure 7.

Supplemental Table Titles and Legends

Supplementary Table 1. Mouse CRISPR TF library design.

Supplementary Table 2. Mouse CRISPR TF library results.

Supplementary Table 3. sgRNAs used for dual-color pluripotency reporter screen, primers and plasmids used in this study.